Computers and Concrete, *Vol. 17, No. 6 (2016)739-760*
DOI: http://dx.doi.org/10.12989/cac.2016.17.6.739

Analysis of punching shear in high strength RC panels– experiments, comparison with codes and FEM results

Ahmed B. Shuraim*, Fahid Aslam[a], Raja R. Hussain[b], and Abdulrahman M. Alhozaimy[c]

Civil Engineering Department, College of Engineering, King Saud University, Riyadh, Saudi Arabia

(Received September 4, 2015, Revised February 6, 2015, Accepted March 8, 2016)

Abstract. This paper reports on punching shear behavior of reinforced concrete panels, investigated experimentally and through finite element simulation. The aim of the study was to examine the punching shear of high strength concrete panels incorporating different types of aggregate and silica fume, in order to assess the validity of the existing code models with respect to the role of compressive and tensile strength of high strength concrete. The variables in concrete mix design include three types of coarse aggregates and three water-cementitious ratios, and ten-percent replacement of silica fume. The experimental results were compared with the results produced by empirical prediction equations of a number of widely used codes of practice. The prediction of the punching shear capacity of high strength concrete using the equations listed in this study, pointed to a potential unsafe design in some of them. This may be a reflection of the overestimation of the contribution of compressive strength and the negligence of the role of flexural reinforcement. The overall findings clearly indicated that the extrapolation of the relationships that were developed for normal strength concrete are not valid for high strength concrete within the scope of this study and that finite element simulation can provide a better alternative to empirical code Equations.

Keywords: punching shear; high strength concrete; coarse aggregate type; silica fume; finite element simulation

1. Introduction

Punching shear, which is a complex three-dimensional problem can cause detrimental failure, unlike flexure it is a sudden failure and can lead to the progressive collapse of complete structures. Several factors have been identified to affect the punching shear strength, among them; compressive strength of concrete, yield strength of steel, ratio of the column size to slab effective depth, shape of the column, and lateral constraints (ACI-ASCE Committee 326, ACI-ASCE Committee 426, ACI-ASCE Committee 445). Most empirical design equation are expressed in

*Corresponding author, Professor, E-mail: ashuraim@ksu.edu.sa
[a]Ph.D. Student
[b]Associate Professor.
[c]Professor

http://www.techno-press.org/?journal=cac&subpage=8 ISSN: 1598-8198 (Print), 1598-818X (Online)

terms of $(f_c')^n$; where n varies between ¼ to ½ and is intended to reflect the tensile or shear strength of concrete under the assumption that the compressive strength is an index of all other mechanical properties. It is questionable whether the extrapolation of the relationships that were established for normal strength concrete remain accurately valid for high strength concrete, due to behavioral differences (ACI 363R-10 2010). It is probably for the validity concern and insufficient data that some codes of practice impose an upper limit on the value of the compressive strength in their design equations (ACI-318, CSA A23.3-04).

The problem of the punching shear has received great attention over several decades because of its importance, (Herzog 1970, Bazant and Cao 1987, Kuang and Morley 1992, Polak 1998, Yamada *et al*. 1992, Alam *et al*. 2009, Moe 1961, Regan 1981, Gardner 1990, 2005, 2011, Marzouk and Hussein 1992, Metwally *et al*. 2008, Hallgren and Kinnunen 1996, Menetrey *et al*. 1997, Ghannoum 1998, Ngo 2001, Menetrey 2002, Albrecht 2002, Salim and Sebastian 2003, Subramanian 2003, Smadi and Yasin 2008, Muttoni 2008, Ahmed and Al Numan 2014, Wosatko, *et al*. 2015, Genikomsou, and Polak 2015, Reis *et al*. 2015, Hassan *et al*. 2015, Kurtoğlu *et al*. 2016. Understanding the punching shear relationship to concrete mechanical properties is a key issue for the safety, serviceability and economy of critical concrete structures.

This study aims to shed some light on punching shear of high strength concrete panels incorporating different types of coarse aggregate and silica fume, in order to assess the validity of the existing code models with respect to the role of compressive and tensile concrete strength. For this purpose, an extended experimental program was carried out involving twenty-one identical panels in geometry and longitudinal reinforcement whereas the variables are the concrete properties. Concrete development involved three type of coarse aggregate and three water/cementitious ratios of 0.25, 0.35, and 0.40. Moreover, some mixtures incorporated ten percent silica fume replacement of cement.

The experimental program was complemented by nonlinear finite element method (FEM) simulation of the panels to provide an insight into the behavior, and to corroborate the experimental findings. The results were analyzed with respect to the variables involved and compared with the results produced by existing code design equations. The findings clearly indicated that the extrapolation of the relationships that were developed for normal strength concrete are not valid for high strength concrete within the scope of this study and that FEM simulation can provide a better alternative to empirical code Equations. Despite the accumulated knowledge in this study and the previous studies, however, some challenges remained unresolved.

2. Experimental program

2.1 Materials

Cement: ASTM Type I, Ordinary Portland cement (OPC), from local cement plant was used. The chemical composition of cement used in this study is presented in Table 1.

Table 1 Chemical composition of cement

SiO_2	Al_2O_3	Fe_2O_3	CaO	MgO	SO_3	Alkalies	C_3S	C_2S	C_3A	C_4AF
19.96	5.99	3.59	62.75	0.59	2.73	0.2	50.6	19.1	9.8	10.9

Table 2 Chemical composition of Micro-silica

SiO_2	Al_2O_3	Fe_2O_3	CaO	MgO	SO_3	Cl	Na_2O
93.20	<0.01	0.05	0.72	0.14	<0.01	0.03	0.07

Table 3 Properties of fine aggregate

Type of aggregate	Specific gravity	Absorption (%)	Dry Rodded bulk density (kg/m^3)	Type
Crushed sand (washed sand)	2.63	1.43	1604.63	Lime stone
White Silica sand	2.63	0.93	1720.27	95% silicates

Silica Fume (SF): Micro silica complying with the requirement of ASTM C 1240 was used. The chemical composition of micro silica is presented in Table 2.

Admixture: Modified poly-carboxylate based high-range water-reducing admixture (HRWR) conforming to the requirements of ASTM C494 type F was used.

Fine aggregate (FA): Two locally available sands with different physical properties were used. Crushed sand has specific gravity of 2.63 and fineness modulus of 4.73 while the other type silica sand has a specific gravity of 2.63 and fineness modulus of 1.78. Combining 35% of crushed and 65 % of silica sand achieved a fineness modulus of 2.74 and acceptable gradation limits. The properties of the fine aggregates are presented in Table 3.

Coarse aggregate (CA): Three types of coarse aggregates of this study were labeled according to the region from which they were obtained, namely: Abha (AB), Makkah (MK) and Riyadh (RY) of Saudi Arabia. Aggregate 'AB' was identified as of metamorphic rock origin composed primarily of quartz along with some biotite contamination and schist layers, especially in the cracks. Aggregate 'MK' was identified as mainly basalt, with mixture of plagioclase and chlorite minerals. It also contains chunks of feldspar in its geometrical formation. Finally, aggregate 'RY' was identified as of sedimentary origin mostly formed of chalky limestone. The petrographic study showed fine grains crystals comprising of mostly calcite minerals with very few quartz grains seen here and there.

While many properties of the aggregate depend entirely on the properties of the parent rock, there are some properties possessed by the aggregate such as particle shape and size, surface texture, and absorption. Table 4 gives some physical properties of coarse aggregate, as tested by standard methods. The chemical elemental analysis of each aggregate was found out by energy dispersive x-rays spectroscopy analysis and presented in Table 5.

Aggregate strengths in terms of impact value determined as per BS 812-112:1990 and Los Angles abrasion value determined as per ASTM C131 are shown in Table 6. Furthermore, the shape factor and volumetric coefficient of coarse aggregate were determined following the work of Sengul *et al*. (2002). The shape factor is defined as the ratio of (maximum dimension of coarse aggregate)/ (minimum dimension of coarse aggregate). If the ratio is greater than 3, then the coarse aggregate is assumed to be a flaky and elongated particle. Consequently, the percentage of the particles greater than 3 is reported in Table 6. On the other hand, another aspect of the shape of coarse aggregate is its volumetric coefficient (H) defined as the ratio of volume of aggregate particle to the volume of aggregate particle considering each particle as complete sphere. It is to be

Table 4 Physical Properties of coarse aggregate

Tests	AB 20mm	AB 10mm	RY 20mm	RY 10mm	MK 20mm	MK 10mm
Bulk Specific gravity (saturated surface dry)	2.77	2.76	2.61	2.62	2.70	2.73
Absorption (%)	0.85	1.82	1.10	1.30	1.15	1.55
Moisture content (%)	0.17	0.32	0.32	0.59	0.49	0.36
Dry rodded bulk density (kg/m^3)	1623	1683	1550	1575	1681	1683

Table 5 Chemical composition of coarse aggregates (percentage)

Type of compound	RY	MK	AB
C (carbon)	13.13	10.24	3.28
O (oxygen)	44.49	40.52	41.95
Na (sodium)	--	3.17	3.24
Mg (Magnesium)	0.21	0.47	0.80
Al (Aluminum)	0.20	5.95	8.06
Si (silicon)	0.42	25.69	33.65
S (sulfur)	--	0.36	---
Cl (chlorine)	--	0.34	---
K (Potassium)	--	1.15	3.17
Ca (Calcium)	41.55	9.63	1.41
Ti (Titanium)	--	0.37	---
Fe (ferrous)	1.21	2.11	4.43

Table 6 Mechanical and shape properties of coarse aggregates

Aggregate type	Impact Value (%)	Abrasion values using 500 Revolutions.	shape factor greater than 3 (%)	Volumetric coefficient H
RY	11.23	23.14	18.72	0.31
MK	4.04	10.84	26.26	0.25
AB	4.48	19.36	47.44	0.25

noted that the volumetric coefficient for cube and sphere are 0.37 and 1.00, respectively. For concrete aggregates, it should not be less than 0.15. For high-performance concretes, the volumetric coefficient should be greater than 0.20 [Sengul *et al*. (2002)].

As a final remark, providing material detailed properties is a useful aid in assessing material quality, in documentation purpose for repeatability and in facilitating comparing a new material with one for which service records are available.

2.2 Mix proportions

Table 7 Mix proportions in a ratio form for all mixes.

w/cm & Cementitious content (kg/m^3)		w/cm=0.25 550 kg/m^3			w/cm=0.35 450kg/m^3			w/cm=0.35 450 kg/m^3			w/cm=0.40 400 kg/m^3		
Designation		W25-S10			W35-S0			W35-S10			W40-S0		
Aggregate designation		RY	MK	AB	RY	MK	AB	RY	MK	AB	RY	MK	AB
Cementitious ratio		1	1	1	1	1	1	1	1	1	1	1	1
SF ratio	kg/kg	0.10	0.10	0.10				0.10	0.10	0.10			
FA ratio	kg/kg	1.22	1.16	1.22	1.62	1.54	1.61	1.58	1.51	1.57	1.91	1.83	1.90
CA ratio	kg/kg	1.92	2.05	2.03	2.35	2.52	2.49	2.35	2.52	2.49	2.64	2.83	2.80
Water ratio	kg/kg	0.27	0.28	0.28	0.38	0.39	0.39	0.38	0.38	0.39	0.43	0.44	0.45
HRWR ratio	Ml/kg	11.00	7.00	6.50	5.00	4.00	3.50	5.50	5.20	5.50	4.00	3.80	3.80
Slump	mm	192	197	192	163	188	175	152	169	170	182	168	182

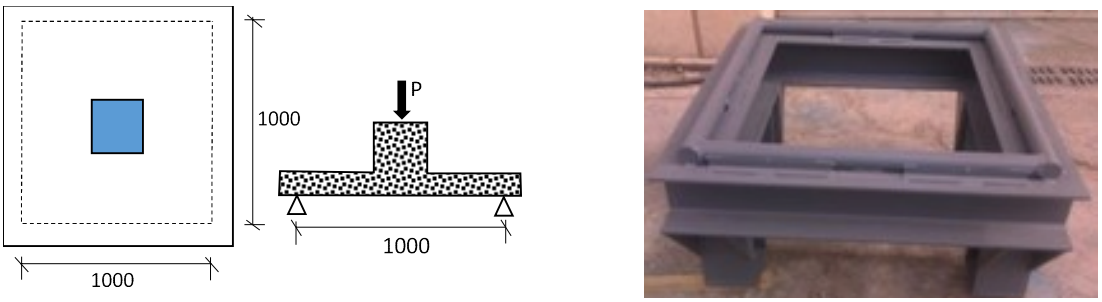

Fig. 1 Schematic arrangement of the specimen and testing frame

In the mix design, cement content, water/cementitious ratio and the slump target of 175±25 mm were chosen based on local experience; however, the remaining steps were performed according to ACI-211.4R-08. The quantities for each mix are presented in Table 7 in ratio form with respect to the total cementitious content. The mass of an ingredient (SF, FA, CA, and water) can be obtained by multiplying the relevant ratio in the table by the cement quantity in the first row, resulting in the quantity of the ingredient in kg/m3.

2.3 Test setup for punching shear

The experimental program consisted of punching shear tests on twenty-one reinforced concrete panels representing twelve concrete mixtures prepared as per Table 7 using three types of coarse aggregates. The overall dimensions of a typical panel were 1200 mm x 1200 mm with a depth of 90 mm. The panel was simply supported along the circumference using the frame shown in Fig. 1. A short cubic column of 150x150x150 mm was cast monolithically with the panel as shown in Fig. 1 and Fig. 2 over which the vertical load was applied.

The RC panels were designed to have no shear reinforcement to easily quantify the contribution of concrete to the shear strength. The RC panel was reinforced with an ASTM A615 Grade 60 rebar mesh composed of 10 mm bars and spaced horizontally as shown in Fig. 2, while the clear cover from the bottom side was 20 mm. The average reinforcement ratio was 0.65 percent in both directions.

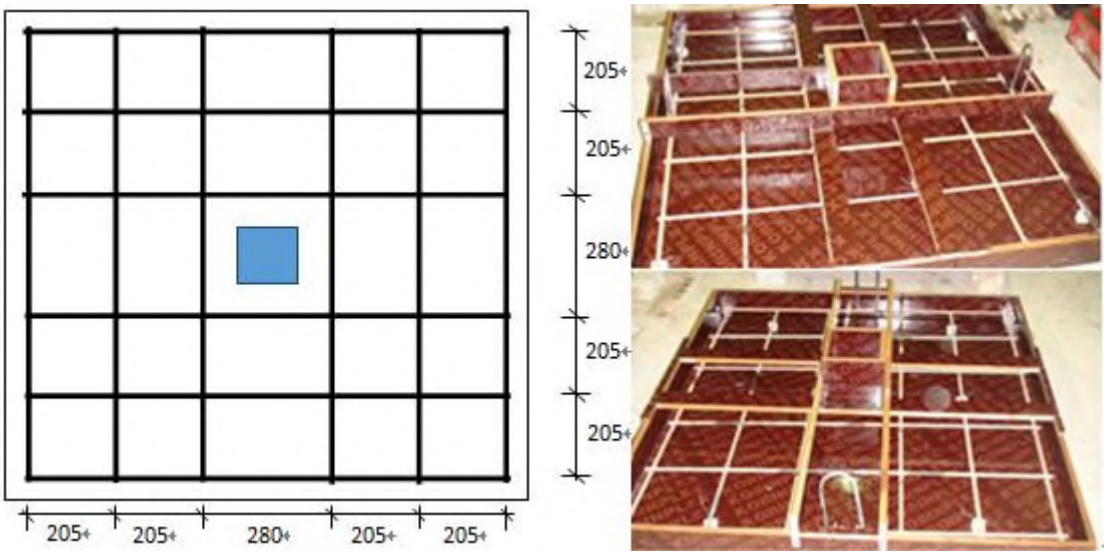

Fig. 2 Schematic and actual arrangement of reinforcement in the slab

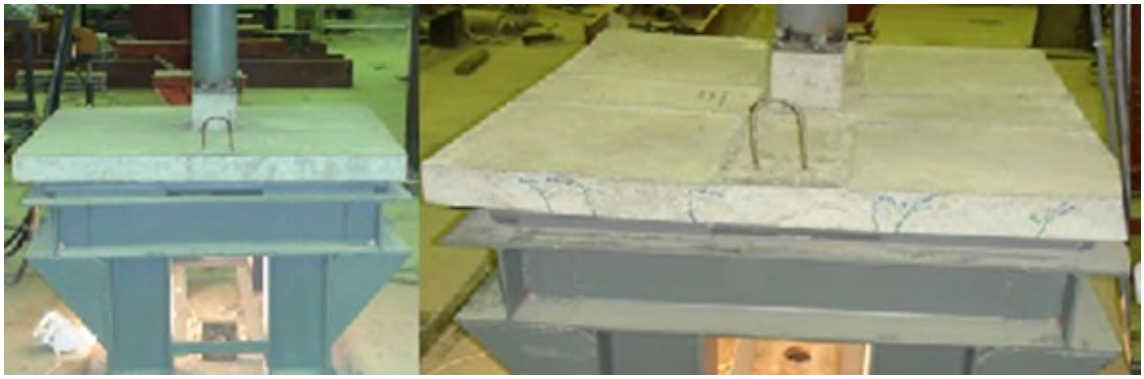

Fig. 3 A panel situated on the supporting frame and subjected to vertical loading

The RC panels were tested under point load applied by pushing the column against the slab as shown in Fig. 3, employing a displacement controlled at a rate of 0.5 mm/minute with the help of closed-loop actuator having a capacity of 500 kN.

3. Experimental findings

The ultimate punching shear forces for the tested panels along with the average concrete compressive strength and the concrete direct tensile strength are presented in Table 8. It is convenient to view the results of each aggregate type along with its tensile and compressive strength. The choice to present the results in this form is intended to explore some fundamental

Table 8 Summary of panel designations and test strength results

no.	Panel/Mix ID	f_c' (MPa) @ 28 days	f_t (MPa) @ 28 days	Ultimate punching shear force (kN)		
				Sample-1	Sample-2	Average
1	RY-W25-S10	102.4	3.03	92	N/A	92
2	RY-W35-S0	70.7	3.51	96	110	103
3	RY-W35-S10	74.6	3.45	115	90	102
4	RY-W40-S0	70.6	2.15	123	125	124
	average					**105**
1	MK-W25-S10	95.2	4.35	82	N/A	82
2	MK-W35-S0	66.8	2.77	112	110	111
3	MK-W35-S10	63.5	3.97	133	111	122
4	MK-W40-S0	67.8	2.75	122	130	126
	average					**110**
1	AB-W25-S10	79.4	3.83	113	N/A	113
2	AB-W35-S0	56.5	3.06	94	110	102
3	AB-W35-S10	65.3	3.55	108	102	105
4	AB-W40-S0	54.2	2.86	95	95	95
	average					**104**

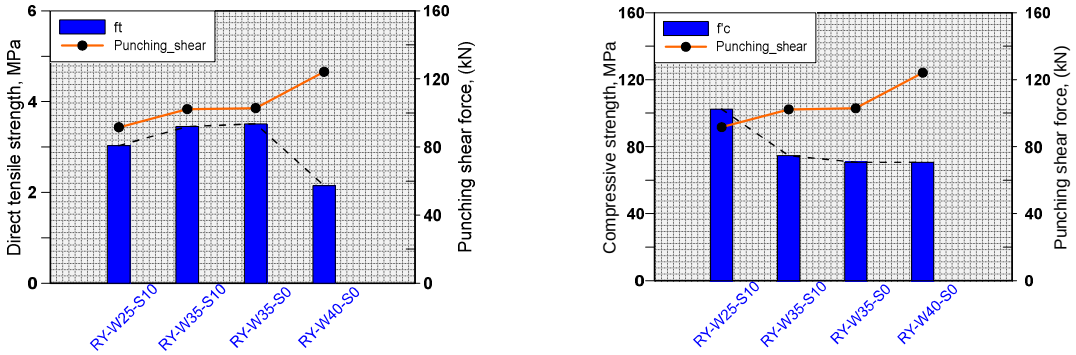

(a) comparison with tensile strength (b) comparison with compressive strength.

Fig. 4 Punching shear force and concrete strength for RY-concrete

relationships. It is recognized in the literature and building codes that punching shear strength is a direct function of square or cube root of compressive strength. Moreover, the direct tensile strength is usually given as a function of the compressive strength. Furthermore, the compressive strength is usually expected to decrease with the increase of the w/cm ratio as per Abrams water-cement ratio formulation, which can be expressed as

$$f_c' = \frac{A}{B^x} \tag{1}$$

Where f_c' stands for the compressive strength of concrete at a designated age, while A and B are empirical constants summarizing various effects. Hence, the comparisons given in Fig. 4

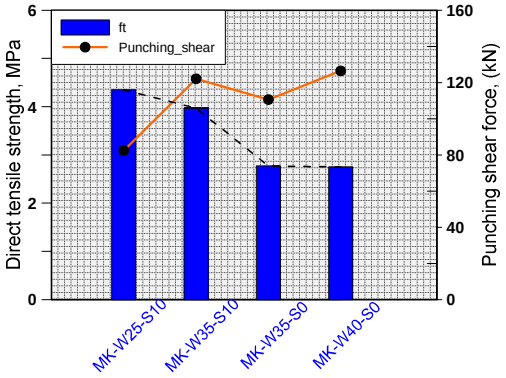

(a) comparison with tensile strength

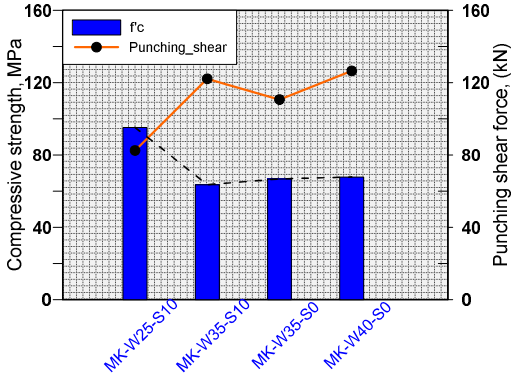

(b) comparison with compressive strength.

Fig. 5 Punching shear force and concrete strength for MK-concrete.

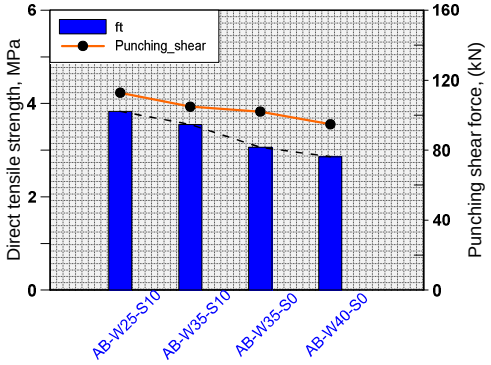

(a) comparison with tensile strength

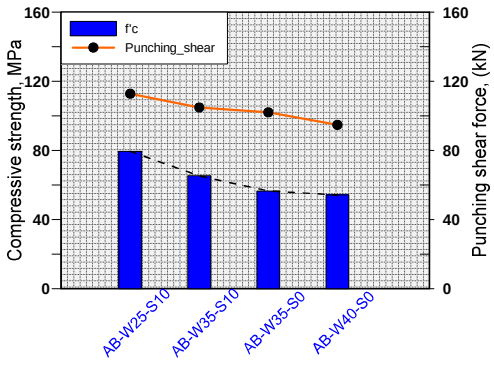

(b) comparison with compressive strength

Fig. 6 Punching shear force and concrete strength for AB-concrete

through Fig. 6 can shed some light on these fundamental relationships as found in this study.

For Ry-concrete, the results are presented in Fig. 4(a) and (b); where the former contains the punching shear force and tensile strength of concrete plotted against the w/cm ratio; while the latter contains the punching shear force and compressive strength of concrete. It is observable that the punching shear and the tensile strength follow similar trend over w/cm ratio of 0.25 and 0.35; however, they diverged at w/cm=0.4 when the punching shear increased unexpectedly. The expected trend is to see both of them follow a descending path as the w/cm ratio increases. From Fig. 4(b), one can observe an increase in the punching shear with the w/cm ratio while the compressive strength follows a decreasing path.

Fig. 5(a) and (b) give the results for MK-concrete. One observation is that the tensile strength decreases in a relatively logical manner with the increase of the w/cm ratio, which is unlike the trend in RY-concrete. It is also observable that no meaningful correlation exist between the punching shear and either the tensile or compressive strength. Finally, Fig. 6 highlights the behavior of AB-concrete, and it shows different performance from the RY and MK concretes. The tensile strength, the compressive strength and the punching shear follow trends that are more logical; they are decreasing with the increase of w/cm in a consistent manner.

Accordingly, the comparisons given in Fig. 4 through Fig. 6 indicate to a large extent that the

Table 9 Punching shear calculation equation from various codes

Code	*shear strength,* $\boldsymbol{v_c}$	size effect, ξ	*Critical perimeter,* b_0
ACI-318	$0.33\sqrt{f_c'}$; $f_c' \leq 70$	-	$b_0 = 2(c_1 + c_2) + 4\,d$
CSA A23.3-04	$0.38\sqrt{f_c'}$; $f_c' \leq 64$	*1300/(1000+d)*	$b_0 = 2(c_1 + c_2) + 4\,d$
EC-2 & CEB-FIP MC 90	$0.18\,(100\rho\, f_{ck})^{\frac{1}{3}}$ $\rho \leq 0.02$	$\left(1 + \sqrt{\frac{200}{d}}\right) \leq 2.0$	$b_0 = 2(c_1 + c_2) + 4\pi\, d$ at 2d
EC-2 &CEB-FIP MC 90 (minimum_shear)	$0.035\sqrt{f_c'}$	$\left(1 + \sqrt{\frac{200}{d}}\right)^{\frac{3}{2}}$	$b_0 = 2(c_1 + c_2) + 4\pi\, d$ at 2d
DIN 1045	$0.21\,(100\rho\, f_{ck})^{\frac{1}{3}}$ $\rho \leq 0.02$	$\left(1 + \sqrt{\frac{200}{d}}\right) \leq 2.0$	$b_0 = 2(c_1 + c_2) + 3\pi\, d$ *at 1.5 d*
BS 8110-97	$0.79\,(100\rho\,)^{\frac{1}{3}}\left(\frac{400}{d}\right)^{\frac{1}{4}}\left(\frac{f_{ck}}{25}\right)^{0.25}$ $f_{ck} \leq 40$		$b_0 = 2(c_1 + c_2) + 12\,d$

correlation between punching shear strength and concrete strength is limited. This finding collaborates the decision by some building codes to impose a maximum limit for concrete strength in their design equations as shown in Table 9. Moreover, it is interesting to notice that keeping all other variables constant, RY and MK concretes produced higher shear capacity at water-cementitious ratio (w/cm) of 0.4 ratio. This phenomenon needs further investigation.

3.1 Effect of aggregate type and silica fume

Considering the average punching shear force from each group, the numeric values are 105 kN, 110 kN, and 104 kN for RY, MK, and AB concrete respectively. These values are similar and do not show a significant variation. The differences among the three groups are in the trend as illustrated by Fig. 4 through Fig. 6. RY-concrete and MK-concrete show overall similarity where the punching shear increases unexpectedly with the increase of w/cm ratio. AB-concrete shows results that are more consistent.

The effect of silica fume may be examined through comparison of W35-S0 and W35-S10 in each group. The use of silica fume caused some moderate effect on MK and AB concretes for punching shear force and tensile strength; but none for RY-concrete. For compressive strength, the use of silica fume caused some moderate effect on RY and AB concretes than for MK concrete.

The literature reveals that the effects of silica fume on the properties of hardened concrete can be directly related to the physical and chemical mechanisms by which silica fume functions. However, ACI 234 states that the contribution of silica fume to strength development after 28 days is minimal. This study did not find a significant contribution of silica fume of shear strength or concrete strength; which to some extent collaborates the literature findings.

4. Comparison of punching shear force: experimental vs. code predictions

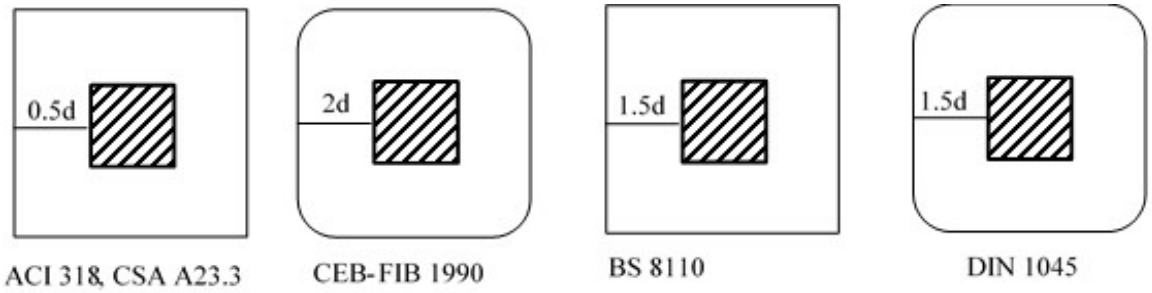

Fig. 7 Critical perimeter shape and location specified in various codes

Table 9 shows a number of code equations for computing the punching shear strength of concrete. The general form may be written as

$$V_c = v_c \times \xi \times b_0 \times d \quad (2)$$

Which is composed of four components as follows:

• Shear strength, $\boldsymbol{v_c}$which is expressed as a function of the compressive strength $(f_c')^n$, where n takes the value of 0.5, 0.33 or 0.25. Moreover, the European code equations (British Code BS 8110-97, CEB-FIP 1990 Model Code, DIN 1045 and Euro Code 2-2003) incorporate a term for the influence of flexural reinforcement ratio, ρ. This indicates different philosophies between the north-American codes and the European codes on the contribution of concrete compressive strength and whether the flexural reinforcement should be included or not.

• Size effect, ξ, is intended to account for the size of the effective depth of the slab and all equations have some form of size effect factor except the ACI-318.

• Critical perimeter, b_0, is the perimeter of the critical section depending upon the equation used; it varies from 0.5 to 2.0 times the effective depth from the face of the column or reaction as shown in Fig. 7.

• d is the average effective flexural depth of the slab.

The variations in the above parameters indicate that they do not reflect the physical reality of the punching phenomenon, but, when properly calibrated, can lead to reasonable predictions. A comparison of test load for all tested panels along with the load calculated using available equations of various design codes is presented in Table 10 numerically. It is to be noted that the design equations are used without the factors of safety presented in each of them. ACI-318 and CSA A23.3-04 tend to overestimate the punching shear strength by exaggerating the contribution of the concrete compressive strength in one hand and by ignoring the role of flexural steel. EC-2 & CEB-FIP MC 90 and DIN 1045 give better prediction except for except two seemingly outlier data points. They seem to be the most suitable equations among the listed equations. The BS 8110-97 gives generally low values but the limit imposed on concrete strength make it only suitable for normal strength concrete. Finally, the minimum shear of EC-2 &CEB-FIP MC 90 gives low values.

Because the ACI-318 and EC-2 are widely used codes of practice, their predictions are represented graphically in Fig. 8(a). It is obvious that ACI-318 is not suitable for punching shear prediction when the panels have low reinforcement ratio while the EC-2 is the best design equation which when considering the factors of safety will lead to a safe design. If we impose a maximum concrete strength of 70 MPa on EC2, it would be more conservative as shown in Fig. 8(b).

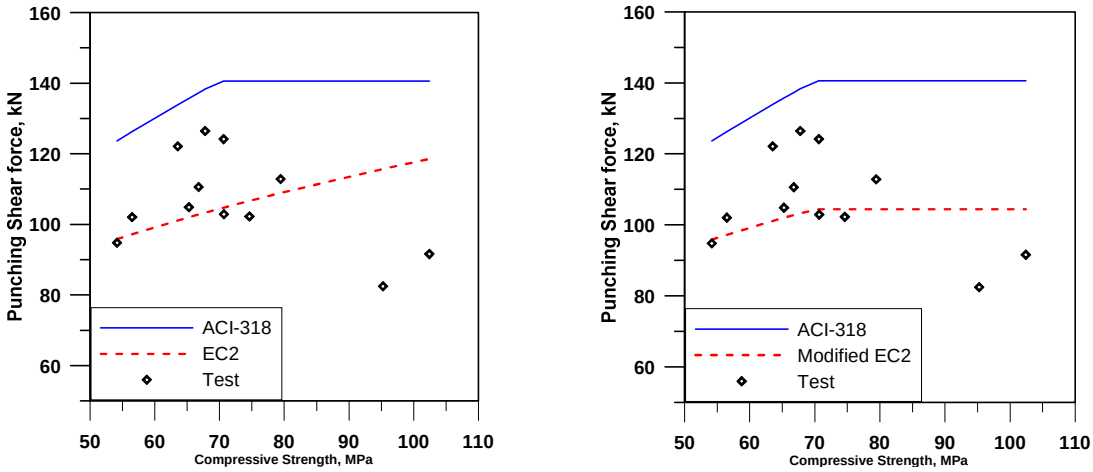

(a) original equations (b) modified EC2

Fig. 8 Comparison of Test load with ACI and EC2 equations: (a); (b).

Table 10 Comparison of experimental and predicted results

MIX ID	ACI/ TEST	CSA/ TEST	EC2/ TEST	EC2_MIN/ TEST	DIN/ TEST	BS/ TEST
RYW25S10	1.53	1.67	1.29	0.89	1.30	1.07
RYW35S10	1.37	1.50	1.04	0.68	1.05	0.96
RYW35S0	1.37	1.49	1.02	0.66	1.02	0.95
RYW40S0	1.13	1.23	0.84	0.54	0.85	0.79
MKW25S10	1.70	1.86	1.40	0.95	1.41	1.19
MKW35S10	1.10	1.25	0.83	0.53	0.83	0.80
MKW35S0	1.24	1.39	0.93	0.59	0.93	0.89
MKW40S0	1.09	1.21	0.82	0.52	0.82	0.77
ABW25S10	1.25	1.36	0.97	0.64	0.97	0.87
ABW35S10	1.29	1.46	0.97	0.62	0.98	0.93
ABW35S0	1.24	1.41	0.95	0.59	0.96	0.96
ABW40S0	1.30	1.49	1.01	0.62	1.02	1.03

5. Comparison of punching shear force: experimental vs. FEM

The tested panels were simulated numerically using finite element procedures in order to gain some insight into the behavior, and to corroborate the experimental findings. In this study, ABAQUS\standard (2009) damage-plasticity model was chosen for modeling concrete behavior. It has been suggested that the coupled damage-plasticity formulation can provide a better representation of salient concrete features (Meyer and okamura 1986, Schnobrich 1985, Chen and Han 1988). The damage-plasticity model in ABAQUS was proposed by Lubliner (1989) and extended by Lee and Fenves (1998) where stiffness degradation due to damage is embedded in the

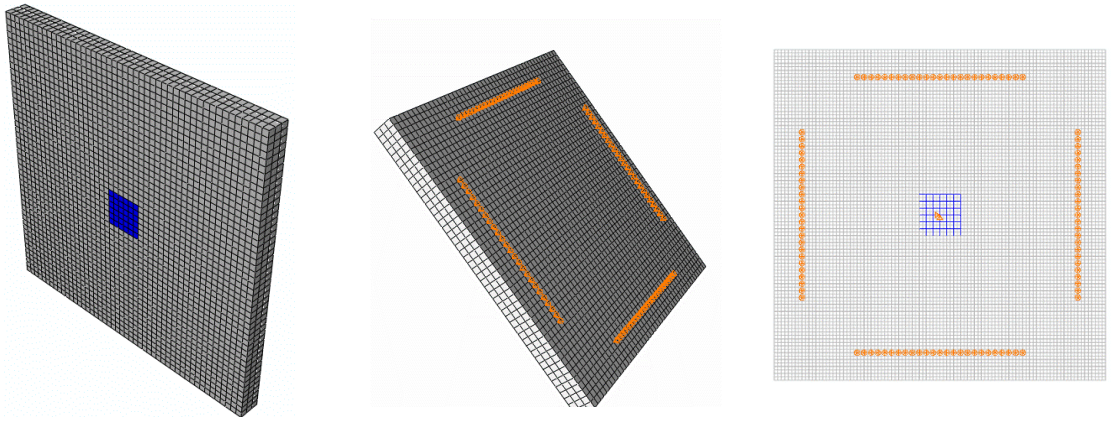

Fig. 9 Mesh and boundary conditions modeling of RC panels

plasticity part of the model using two independent scalar damage parameters.

The post-peak in tension can be represented in different forms, among them the fictitious crack model by Hillerborg (1985a, 1985b), which is characterized by three key parameters: the specific energy dissipated after the localization in the cracked region; the tensile strength in direct tension; and, the shape assumed for the softening branch. The fracture energy-cracking criterion has been employed instead of strength failure criterion in order to minimize the superficial dependence on the chosen finite element.

Despite the advancement in software development, it is essential to recognize that finite element models comprise various theories, elements and procedures where some limitations, shortcomings and complexity were reported (Vecchio 2001, Vecchio *et al.* 2004). Numerical simulation models for structure behavior are affected by the choices made in their spatial modeling, material modeling, element characteristics, and solution procedures. Among the challenges in modeling concrete structures is the numerical modeling of cracking where two main approaches have been considered (ACI-446 1997, Belytschko and Black 1999, Simone *et al.* 2003, Sain and Chandra 2007, de Borst 2002). Discrete approach represents a crack as a geometrical discontinuity; however, its main drawback is that one needs to know location of an expected crack and the direction along which it propagates (Sain and Chandra 2007). On the contrary, smeared crack through damage mechanics offers the essential advantage of predicting the location of this critical flaw.

5.1 Model assumptions

For punching shear, the nature of the problem is complex and requires three-dimensional modeling for geometrical and material considerations. Spatially, concrete was modeled through solid three-dimensional (3D) elements (C3D8), whereas 2-node truss elements (T3D2) were employed for rebars; the bond between the two materials was assumed perfect at their common nodal points. The influence of element type was investigated in the parametric study where concrete was modeled by quadratic 20-node elements (C3D20) while rebars were modeled by 3-node truss elements (T3D3). As shown in Fig. 9, a fine mesh was selected where the depth is represented by three solid layers of 0.03 m, while the plan was meshed every 0.025 m, resulting in

almost cubic elements. The size of the mesh in the panel surface was chosen to allow defining the loading area and the boundary condition properly.

For the effect of supporting frame, nodal points at the bottom surface were constrained against moving vertically downward except at the corners as shown in Fig. 9. Corner nodes that tended to move vertically upward were left unconstrained to facilitate their free movement. Loading was applied incrementally and iteratively as a downward pressure over the marked area in Fig. 9 which represents the column sectional area. The number of increments varied from case to case, but in general, it exceeded a hundred increments as determined by the default scheme of the program until equilibrium ceased to exist. The only exception was that the self-weight of the panel was applied prior to the pressure load over two increments.

The material input parameters for the damage-plasticity model of concrete include uniaxial compression curve, uniaxial tensile strength, Poisson's ratio, modulus of elasticity, dilatancy angle, and fracture energy. These parameters were defined as per available test data as well as from appropriate constitutive models from the technical literature [Shuraim-2006; Shuraim-2012]. Some values were kept constant, including: Poisson's ratio (0.2), dilatancy angle (56°), even though the effect of the dilatancy angle was examined in the parametric study by considering different angles along with the viscosity parameter.

The fracture energy, G_f, was expressed by Eq. (3) (fib Bulletin 42 2008).

$$G_f = 110 \left(\frac{f_c'}{10}\right)^{0.18} \tag{3}$$

Direct tensile strength, f_t' (MPa) was taken as

$$f_t' = 0.25 \sqrt{f_c'} \tag{4}$$

Post-cracking tensile curve for concrete was defined by Eq. (5) (Murthy *et al*. 2009), where n is a coefficient taken as 3.

$$f_t = f_t' \left(1 - \frac{x}{d_0}\right)^n; \qquad d_0 = \frac{G_f(n+1)}{f_t'} \tag{5}$$

For uniaxial compression stress-strain curve, the following expression was adopted following Carreira, and Chu (1985)

$$\frac{f_c}{f_c'} = \frac{\beta \frac{\varepsilon}{\varepsilon_0}}{\beta - 1 + \left(\frac{\varepsilon}{\varepsilon_0}\right)^{\beta}}; \quad \text{where } \beta = \frac{1}{1 - \frac{f_c'}{\varepsilon_0 E_c}} \tag{6}$$

Where the strain at maximum stress was defined by Ahmed (1981) as;

$$\varepsilon_0 = 0.001648 + 0.0000165\, f_c' \tag{7}$$

The modulus of elasticity for concrete, E_c (MPa) was given by ACI-363, as

$$E_c = 3300\sqrt{f_c'} + 6900 \tag{8}$$

The uniaxial stress-strain curve is shown in Fig. 10(a); while, Fig. 10(b) shows the tensile post cracking assumptions. Steel strength was assumed to follow a bi-linear elastic-plastic model and a perfect bond was assumed between concrete and steel.

Table 11 Simulation cases: assumptions and punching shear strength

Case	f_c'(MPa)	f_t'(MPa)	E_c(GPa)	ρ	elements	G_f(N/m)	$V_u(kN)$	ψ
Case 1	59	2.236	29.5	0.0065	C3D8	0.160	102	56
Case 2	80	2.236	33.5	0.0065	C3D8	0.160	102	56
Case 3	59	3.354	29.5	0.0065	C3D8	0.160	112	56
Case 4	59	4.472	29.5	0.0065	C3D8	0.160	119	56
Case 5	59	2.236	29.5	0.0130	C3D8	0.160	148	56
Case 6	59	2.236	29.5	0.0065	C3D20	0.160	107	56
Case 7	59	2.236	29.5	0.0065	C3D8	0.160	96	45
Case 8	59	2.236	29.5	0.0065	C3D8	0.160	103	45*

*For Case 8, a dilatancy angle of 45 was associated with a viscosity parameter of 0.01.

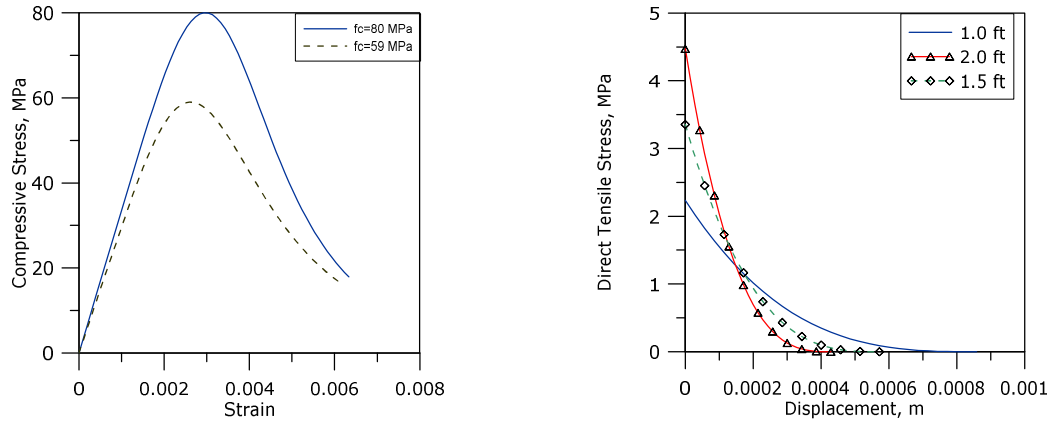

(a) Compressive curves (b): post-peak tensile curves

Fig. 10 Compressive and tensile assumptions of concrete

5.2 Parametric study cases

The purpose of the parametric study was to assess the influence of some key parameters including materials and modeling assumptions. For concrete strength, four cases were considered as per Table 11 by varying concrete strength in tension and compression in order to determine their influence on the punching shear capacity of the panels. Case 1 and 2 differ by the compressive strength where the value in case 2 is 35 percent higher than that in case 1. Three values of tensile strength are considered in cases 1, 3, and 4 where the value of f_t' in case 1 is determined by Eq. (4).

In Case 5 the flexural reinforcement ratio was doubled from the actual value to explore its effect. Case 6, examine a modeling assumption where concrete was modeled by quadratic 20-node elements (C3D20) along with 3-node truss elements (T3D3) for rebars instead of the linear 8-node elements (C3D8) and 2-node truss elements (T3D2), respectively. In Cases 7 and 8, two values of dilatancy angle were considered. Finally, case 9 combined the effect of dilatancy angle along with a viscosity parameter of 0.01; noting that the viscosity parameter for all other cases was remained as the default value of zero.

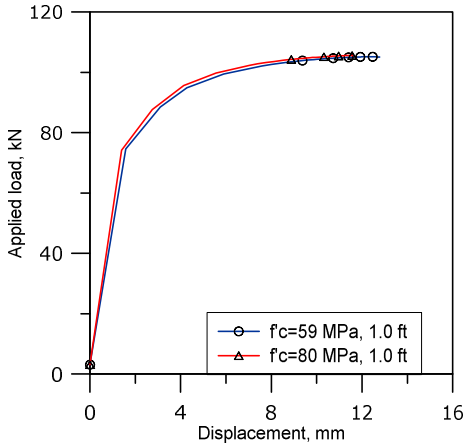

Fig. 11 Load deflection curves for 59 and 80MPa, compressive strengths

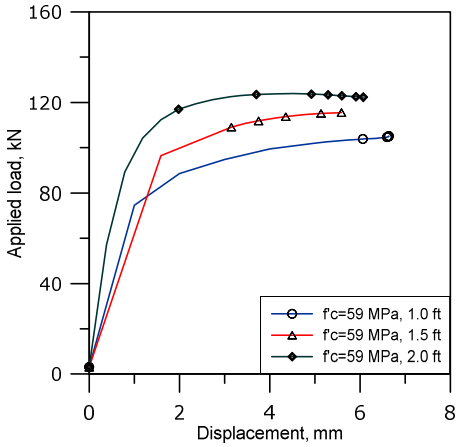

Fig. 12 Load deflection curves for different tensile strengths

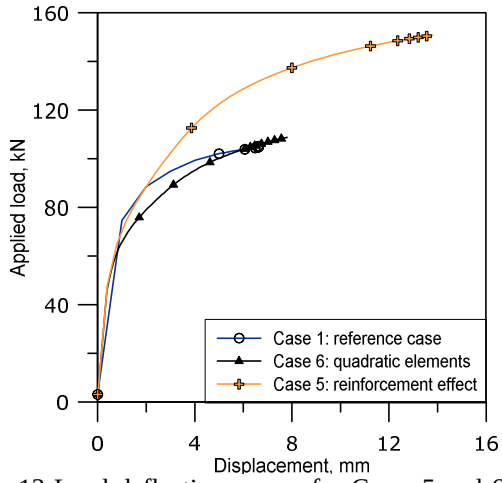

Fig. 13 Load deflection curves for Cases 5 and 6 in comparison with the reference case

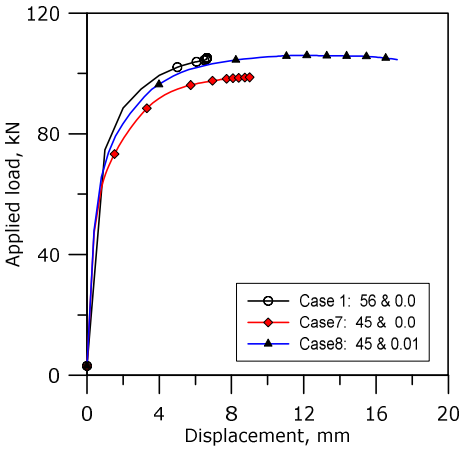

Fig. 14 Load deflection curves for combinations of dilatancy angle and viscosity parameter

5.3 Discussion of numerical results

The results of the numerical analyses of the nine modeling cases provided some insight into the effects of materials on the panel punching shear capacity as well as the effects of some modeling assumptions. Comparing Cases 1 and 2 in Table 11, it is shown that increasing the concrete strength from 59 to 80 MPa was associated with negligible increase in the shear capacity, as depicted by in Fig. 11, when the tensile properties remained constant. This finding from the FEM corroborated the test results in indicating that the compressive strength was not as significant in its direct contribution. It may be interpreted that punching shear failure was controlled by other modes and strengths prior to reaching the concrete compression capacity.

The effect of the assumptions on tensile strength under constant fracture energy is presented in Fig. 12 for Cases 1, 3, and 4 of Table 11. Increasing the tensile strength from a base value given by Eq. (4) by 50 percent and 100 percent caused an increase in the punching shear by 10 and 17

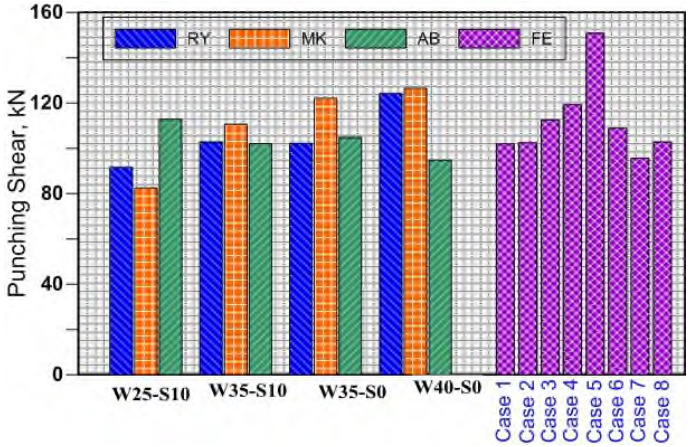

Fig. 15 Comparison of experimental results with the FEM results

percent, respectively.

Comparing Cases 1 and 5 in Table 11, it is shown that increasing the flexural reinforcement by 100 percent would result in an increase of 48 percent in the punching shear. Consequently, this finding may be interpreted to indicate the importance of increasing the minimum flexural reinforcement in panels in order to utilize the potential benefits of high strength concrete.

The remaining cases are pertinent to modeling assumptions. Comparing Cases 1 and 6 is intended to examine the effect of element type and the adequacy of mesh refinement. A 20-node concrete solid element has three layers of integration points, in any direction; while an 8-node element has two layers of integration points. Hence, using a 20-node element has provided substantial mesh refinement in terms of integration points in comparison to an 8-node element model when the number of solid elements are the same. In particular, while the panel depth was represented by 3 rows of solid elements, it is represented numerically by six and nine integration-point layers when modeled by 8-node elements and 20-node elements, respectively, constituting a 50 percent improvement. Therefore, it is plausible to interpret the seven percent difference in the punching shear forces between Cases 1 and 6, as an indication that the model meshing was sufficiently fine.

Cases 7 and 8 addressed two assumptions in the damaged-plasticity model; namely, dilatancy angle and viscosity parameter. In Cases 1 to 6, the dilatancy angle was taken as 56 while the viscosity parameter remained at its default value of zero. Comparing cases 1 and 7 shows that reducing dilatancy angle to 45 resulted in a lower punching shear strength of the panels, by 6 percent. However, when combined the effect of dilatancy angle along with a viscosity parameter of 0.01 (Case 8), the punching shear became approximately as for Case 1 (103 kN); noting that the viscosity parameter for all other cases was remained as the default value of zero.

A summary of the comparison of the test results along with the finite element numerical results is presented in Fig. 15. The overall average of all experimental shear value was 108 kN with standard deviation of 13.7 kN and a coefficient of variations of 12.7 percent; while the finite element numerical punching shear varies between 104 and 121 with an average value of 110 kN for the material Cases 1 to 4. Considering the unavoidable scatter in punching shear as known in the literature and indicated in this study, the numerical results and the test results are in general agreement.

Fig. 16 physical cracking at the bottom of the tested RC panel

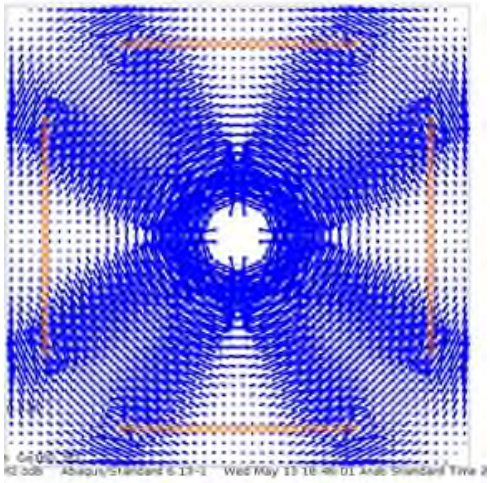

Fig. 17 Maximum plastic tensile concrete strain

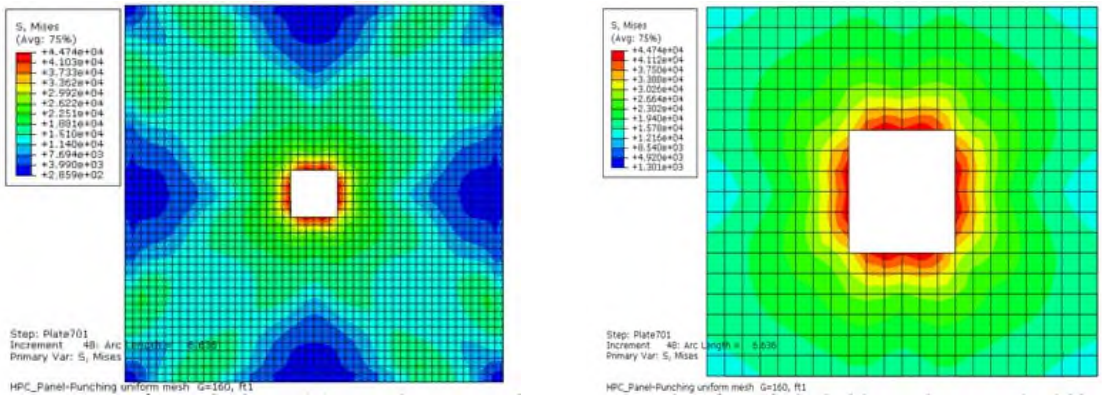

Fig. 18 Misses stress around the loaded column showing stress concentration with elliptical shape

5.4 Concrete cracking and numerical tensile strains

In addition to the numerical comparison, a reasonable matching of the cracking patterns in the tested panels with the visual representation by the model can provide a level of confidence in the simulation process. A typical panel is shown in Fig. 16. Major cracking propagates on the bottom side of the tested panels following a diagonal path connecting the loaded area towards the corners, but with some angular offset from the corner point. Cracks that are perpendicular to the sides are minors.

The numerical model does not produce actual physical cracks, however, maximum plastic strains can usually be interpreted to show the potential cracking patterns. Fig. 17 shows the maximum plastic tensile concrete strain in a symbolic form where the length of the arrowed- lines is an indication of the magnitude and the potential crack is to develop perpendicular to the line direction. A thorough examination of the direction of these symbolic arrows indicates good qualitative agreement with the observed cracks in the tested panels.

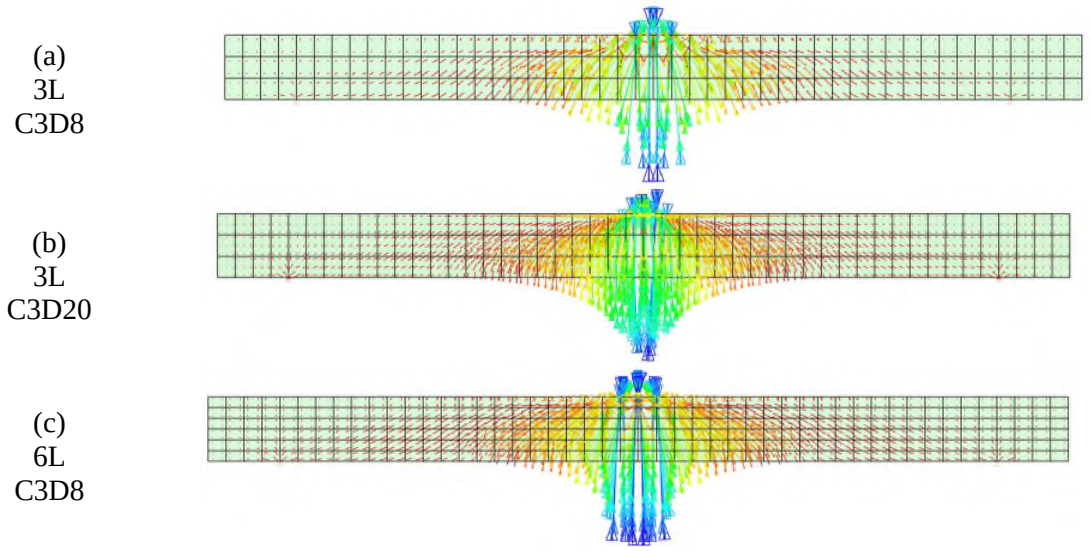

Fig. 19 Compressive principal strain distributions on a vertical section for different cases

5.5 Identifying critical perimeter

Referring to Eq. (2) which described the general equation of various codes as $Vc = v_c \times \xi \times b_0 \times d$, where b_0 is the critical perimeter. This critical perimeter has different shape and location by various codes, as illustrated in Table 9 and in Fig. 7. It is usually situated between 0.5 to 2 times the effective depth from the edge of the loaded area, as shown in Fig. 7. The shorter perimeter can be justified by the existing of cracking patterns and concentration of shear stresses; on the other hand, the advantage of considering a large critical perimeter is to avoid the complex local shear stress so that the influence of the geometry of the loaded area could be neglected. Accordingly, the latter condition leads to a robust failure criterion for punching without shear reinforcement (FIB Bulletin No.12 2001).

The shape and location of the critical perimeter in view of the distribution of stress intensity can be visualized qualitatively from Fig. 18, which shows the state of stresses in terms of Mises stresses distribution contour. The high values surrounding the loading area reflects the complex state of stress of normal and shearing stresses. However, the stress concentrations fade away within less than 2d from the face of load area, as indicated by the contour lines. Moreover, the shape of the banded stress area is taking an elliptical shape. This elliptical shape resembles to a large extent the perimeter shape proposed by the DIN and EC2.

Finally, the compressive principal strain distributions on a vertical section at the horizontal center of the slab are presented in Fig. 19. Figs. 19 (a to b) show the strain distribution for case 1 and case 6 from which the shape of the punching cone is visible. Fig. 19(c) shows the strain distribution for case 1 when the depth is represented by six layers of solid elements instead of three The distributions of strains for the three cases are similar in simulating the potential punching cone boundaries.

6. Conclusions

This paper reports on punching shear behavior of twenty-one full-scale reinforced concrete panels, investigated experimentally and through finite element simulation. The aim of the study was to shed some light on punching shear of high strength concrete panels incorporating different types of aggregate and silica fume, in order to assess the validity of the existing code models with respect to the role of compressive and tensile strength of high strength concrete. The main findings of the study may be summarized as follows:

• The overall average values of the ultimate punching shear for the mixes of three types of coarse aggregate are of similar magnitude. This shows that, the punching behavior is independent of aggregate properties, such as gradation, strength, shape factor, surface texture, and volumetric coefficient.

• The punching shear capacity of the RC panels did not show clear correlation with the compressive strength or tensile strength of concrete. In addition, the incorporation of silica fume did not show much positive effect on the punching shear capacity of the tested panels in any group.

• The prediction of the punching shear capacity of high strength concrete using the equations listed in this study, point to a potential unsafe design, especially those of ACI-318 and CSA-A23.3-04. This may be a reflection of the overestimation of the contribution of compressive strength and the negligence of the role of flexural reinforcement. On the other hand, European code EC-2, CIB-FIB and British code showed more tendency to conservative predictions for most of the test results, except two seemingly outlier data points. This study recommends using EC-2 equation with limitation of the maximum compressive strength to 70 MPa.

• The numerical simulation of the panels under a systematic parametric investigation provided an insight into the behavior, and corroborated the experimental findings with respect to the role of compressive and tensile strength of high strength concrete on the punching shear of the tested panels.

In summary, the findings clearly indicated that the extrapolation of the relationships that were developed for normal strength concrete are not valid for high strength concrete within the scope of this study and that finite element simulation can provide a better alternative to empirical code Equations.

Acknowledgment

The National Plan funded this Project for Science, Technology and Innovation (MAARIFAH), King Abdulaziz City for Science and Technology, Kingdom of Saudi Arabia, Award number ADV-208.

References

ABAQUS (2009), *Users manuals and theory manual version 6.10, Hibbitt*, Karlsson & Sorensen, Inc., Pawtucket, RI, USA.

ACI 211.4R (2008), *Guide for selecting proportions for high-strength concrete using portland cement and other cementitious materials*, American Concrete Institute; Farmington Hills, MI,

USA.
ACI 212.3R (2010), *Report on chemical admixture for concrete*, American Concrete Institute; Farmington Hills, MI, USA.
ACI 234R-06 (2012), *Guide for the Use of silica fume in concrete*, American Concrete Institute; Farmington Hills, MI, USA.
ACI 318M-11 (2011), *Building code requirements for structural concrete and commentary*, American Concrete Institute, Farmington Hills, MI, USA.
ACI 363R-10 (2010), *State-of-the-art report on high strength report*, American Concrete Institute; Farmington Hills, MI, USA.
ACI 446(1997), *Finite element analysis of fracture in concrete structures: State-of-the-Art (ACI 446.3R-97)*, American Concrete Institute; Farmington Hills, MI, USA.
ACI-ASCE Committee 326 (1962), "Shear and diagonal tension," ACI J., **59**(1), 1-30.
ACI-ASCE Committee 426 (1987), *The shear strength of reinforced concrete members, Part 4 of ACI Manual of Concrete Practice*, ACI; Farmington Hills, MI, USA.
ACI-ASCE Committee 445 1998), "Recent approaches to shear design of structural concrete", *J. Struct. Eng.*, **124**(12), 1375-1417.
Ahmed, F.R. and Al Numan, B.S. (2014), "Failure characteristics and critical punching perimeter of High strength concrete panels", *Int. J. Eng. Trend. Tech.*, **13**(8).
Ahmed, S.H. (1981), "Properties of confined concrete subjected to static and dynamic loading", Ph.D.Thesis, University of Illinois at Chicago, USA.
Jahangir Alam, A.K.M., Amanat, K.M. and Seraj, S.M. (2009), "Experimental investigation of edge restraint on punching shear behaviour of RC slabs", *IES J. Part A: Civil Struct. Eng.*, **2**(1), 35-46.
Albrecht, U. (2002), "Design of flat slabs for punching–European and North American practices", *Cement Concrete Compos.*, **24**(6), 531-538.
Bažant, Z.P. and Zhiping, C. (1987), "Size effect in punching shear failure of slabs", ACI Struct. J., **84**(1), 44-53.
Belytschko, T. and Black, T. (1999), "Elastic crack growth in finite elements with minimal remeshing", *Int. J. Numer. Method. Eng.*, **45**(5), 601-620.
BS 8110-97(1997), *Structural use of concrete, part 1: code of practice for design and construction*, British Standards Institution, London, UK.
Carreira, D.J. and Kuang-Han, C. (1986), "Stress-strain relationship for reinforced concrete in tension", *ACI J.*, **83**(3), 21-28.
CEB-FIP MC90(1993), *Design of concrete structures-CEB-FIP Model Code 1990*, Thomas Telford, London, UK.
Chen, W.F. and Da-Jian, H. (1988), *Plasticity for structural engineers*, Springer-Verlag, New York, USA.
CSA A23.3-04(2004), *Design of concrete structures*, Canadian Standards Association, Rexdale, ON, Canada, 358.
de Borst, R. (2002), "Fracture in quasi-brittle materials: a review of continuum damage-based approaches", *Eng. Fract. Mech.*, **69**(2), 95-112.
DIN 1045-1(2007), *Plain, reinforced and prestressed concrete structures-part 1: design and construction*, Normenausschuss Bauwesen (NABau) im DIN Deutsches Institut für Normung e.V.Beuth Verl.Berlin.
Eurocode 2(2004), *Design of concrete structures, part 1-1: general rules and rules for buildings (EN1992-1-1)*, European Committee for Standardization, Brussels, Belgium.

Fib Bulletin 42(2008), "Constitutive modelling of high strength / high performance concrete, State-of-art report", *International Federation for Structural Concrete (fib)*, Lausanne, Switzerland.

FIB Bulletin No.12 (2001), *Punching of structural concrete slabs*, fib Bulletin 12, Lausanne, Switzerland.

Gardner, N.J. (1990), "Relationship of the punching shear capacity of reinforced concrete slab with concrete strength", *ACI Struct. J.*, **87**(1), 66-71.

Gardner, N.J. (2005), "ACI 318-05, CSA A23.3-04, Eurocode 2 (2003), DIN 1045-1 (2001), BS 8110-97 and CEB-FIP MC 90 Provisions for Punching Shear of Reinforced Concrete Flat Slabs" ACI Special Publication, SP-232, 1-22.

Gardner, N.J. (2011), "Verification of punching shear provisions for reinforced concrete flat slabs", *ACI Struct. J.*, **108**(5), 572-581.

Ghannoum, C.M. (1998), "Effect of high strength concrete on the performance of the column-slab specimens", MSc. Thesis, McGill University, Canada.

Genikomsou, A.S. and Maria, A.P. (2015), "Finite element analysis of punching shear of concrete slabs using damaged plasticity model in ABAQUS", *Eng. Struct.*, **98**, 38-48.

Hassan, A.M.T., Mahmud, G.H., Jones, S.W. and Whitford, C. (2015), "A new test method for investigating punching shear strength in Ultra High Performance Fibre Reinforced Concrete (UHPFRC) slabs", *Compos. Struct.*, **131**, 832-841.

Hallgren, M. and Kinnunen, S. (1996), "Increase of punching shear capacity by using high-strength concrete", *Proceedings of the 4th International Symposium On Utilization of High-strength/High-performance Concrete*, Paris, May.

Herzog, M. (1970), "A new evaluation of earlier punching shear tests", *Concrete*, **4**(12), 448-450.

Hillerborg, A. (1985a), "The theoretical basis of a method to determine the fracture energy GF of concrete", *Mater. Struct.*, **18**(4), 291-296.

Hillerborg, A. (1985b), "Results of three comparative test series for determining the fracture energy GF of concrete", *Mater. Struct.*, **18**(5), 407-413.

Kuang, J.S. and Morley, C.T. (1992), "Punching shear behavior of restrained reinforced concrete slabs", *ACI Struct. J.*, **89**(1), 13-19.

Kurtoğlu, E.A., Abdulkadir, Ç., Hasan, M.A., Mehmet, E.G. and Mahmut, B. (2016), "Reliability-based modeling of punching shear capacity of FRP-reinforced two-way slabs", *Comput. Concrete*, **17**(1), 87-106.

Lee, J. and Gregory L.F. (1998), "Plastic-damage model for cyclic loading of concrete structures", *J. Eng. Mech.*, **124**(8), 892-900.

Lubliner, J., J. Oliver, S. Oller and E. Oñate (1989), "A Plastic-damage model for concrete", *Int. J. Solid. Struct.*, **25**(3), 229-326.

Marzouk, H. and Hussein, A. (1992), "Experimental investigation on the behavior of high-strength concrete slabs", *ACI Struct. J.*, **88**(6), 701-713.

Menetrey, P. (2002), "Synthesis of punching failure in reinforced concrete", *Cement Concrete Compos.*, **24**(6), 497-507.

Menetrey, P., Walther, R., Zimmermann, T., William, K.J. and Regan, P.E. (1997), "Simulation of punching failure in reinforced-concrete structures", *J. Struct. Eng.*, **123**(5), 652-658.

Metwally, I.M., Issa, M.S. and El-Betar, S.A. (2008), "Punching shear resistance of normal and high-strength reinforced concrete flat slabs", *Civil Eng. Res. Mag.*, **30**(3), 982-1004.

Meyer, C. and Okamura, H. (1986), "Finite element analysis of reinforced concrete structures", *Proceedings Of The Seminar Sponsored By The Japan Society For The Promotion Of Science*

And The U.S. National Science Foundation, Tokyo, May.
Moe, J. (1961), "Shearing strength of reinforced concrete slabs and footings under concentrated loads", Bulletin D47, Portland cement association, Research and Development Laboratories.
Murthy, R.C., Palani, G.S. and Nagesh, R.I. (2009), "State-of-the-art review on fracture analysis of concrete structural components", *Sadhana*, **34**(2), 345-367.
Muttoni, A. (2008), "Punching shear strength of reinforced concrete slabs without transverse reinforcement", *ACI Struct. J.*, **105**(4), 440-450.
Ngo, D.T. (2001), "Punching shear resistance of high-strength concrete slabs", *Electr. J. Struct. Eng.*, **1**(1), 52-59.
Polak, M.A. (1998), "Modelling punching shear of reinforce concrete slabs using layered finite elements", *ACI Struct. J.*, **95**(1),71-80.
Reis, N., de Brito, J., Correia, J.R. and Arruda, M.R. (2015), "Punching behaviour of concrete slabs incorporating coarse recycled concrete aggregates", *Eng. Struct.*, **100**, 238-248.
Sain, T. and Kishen, J.M.C. (2007), "Energy-based equivalence between damage and fracture in concrete under fatigue", *Eng. Fract. Mech.*, **74**(15), 2320-2333.
Salim, W. and Sebastian, W.M. (2003), "Punching shear failure in reinforced concrete slabs with compressive membrane action", *ACI Struct. J.*, **100**(4), 471-479.
Schnobrich, W.C. (1985), "The role of finite element analysis of reinforced concrete structures", *Proceedings of the Seminar Sponsored by the Japan Society for the Promotion of Science and the U.S.National Science Foundation*, Tokyo, Japan.
Sengul, O., Tasdemir, C. and Tasdemir, M.A. (2002), "Influence of aggregate type on mechanical behavior of normal-and high-strength concretes", *Mater. J.*, **99**(6), 528-533.
Shuraim, A.B. (2006), "Three-dimensional non-linear modelling aspects of a full-scale reinforced concrete banded-joist floor", *Proceedings of the Eighth International Conference on Computational Structures Technology*, Civil-Comp Press, Stirlingshire, September.
Shuraim, A.B. (2012), "Numerical forensic model for the diagnosis of a full-scale RC floor", *Latin American J. Solid. Struct.*, **9**(2), 1-19.
Simone, A., Wells, G.N. and Sluys, L.J. (2003), "From continuous to discontinuous failure in a gradient-enhanced continuum damage model", *Comput. Method. Appl. Mech. Eng.*, **192**(41), 4581-4607.
Smadi, M.M. and Yasin, I.B. (2008), "Behavior of high-strength fibrous concrete slab–column connections under gravity and lateral loads", *Constr. Build. Mater.*, **22**(8), 1863-1873.
Subramanian, N. (2003), "Shear strength of high strength concrete beams: Review of the codal provisions", *The Ind. Concrete J.*, **77**(5), 1090-1094.
Vecchio, F.J. (2001), "Non-linear finite element analysis of reinforced concrete: at the crossroads", *Struct. Concrete*, **2**(4), 201-212.
Vecchio, F.J., Bentz, E.C. and Collins, M.P. (2004), "Tools for forensic analysis of concrete structures", *Comput. Concrete*, **1**(1), 1-14.
Wosatko, A., Pamin, J. and Polak, M.A. (2015), "Application of damage–plasticity models in finite element analysis of punching shear", *Comput. Struct.*, **151**, 73-85.
Yamada, T., Nanni, A. and Endo, K. (1992), "Punching shear resistance of flat slabs: Influence of reinforcement type and ratio", *ACI Struct. J.*, **89**(5), 555-563.

CC